Arabian Journal for Science and Engineering (2022) 47:14989–15000
https://doi.org/10.1007/s13369-022-06638-3

RESEARCH ARTICLE-SYSTEMS ENGINEERING

Impedance Control with Bounded Actions for Human–Robot Interaction

Victor I. Ramírez-Vera[1] · Marco O. Mendoza-Gutiérrez[1] · Isela Bonilla-Gutiérrez[1]

Received: 6 September 2021 / Accepted: 23 January 2022 / Published online: 19 February 2022

Abstract
Human–robot interaction tasks have seen an increased interest in recent years, leading to the need for new proposals both for the design of new robotic systems and for their control and security schemes. In this regard, this work proposes a first approach to impedance control for robot manipulators with bounded inputs which aims to achieve safe human–robot interaction. The proposed scheme has a nonlinear proportional–derivative structure with compensation (PD+) based on the robot model, makes use of generalized saturation functions to generate bounded control actions, and includes an external torque compensation term based on the user's electromyographic information. One of the main advantages of this proposal is that the human–robot interaction is defined in the joint space, which avoids singularities, since the robot works within its natural coordinates and the torque applied by the user is estimated at a joint level. The advantage of the novel control scheme can be demonstrated by the stability analysis of the closed-loop system equilibrium point, as well as by comparative analysis of the simulation results.

Keywords Bounded inputs · Impedance control · Lyapunov stability · Robot manipulator

1 Introduction

Robotic manipulation systems are very popular in different types of applications [1,2], mainly in industry; however, nowadays other areas such as medical services are taking advantage of these systems in human–robot interaction tasks [3]. Among the main medical applications are rehabilitation and assistance due to the repetitive nature of the therapies, and because the recovery progress of a patient is directly related to the quality and quantity of the repetitions carried out during the therapy process [4].

Furthermore, research into the design of control algorithms for robot manipulators has been in constant development during recent decades. However, many of these control algorithms assume that robotic actuators can provide any force/torque value, which is impossible in practice since actuators can only supply up to a maximum torque value and generate movement up to a maximum speed [5]. In human–robot interaction tasks, if the actuators operate outside such limit values, the robot could harm the human user or itself. Therefore, for reliable and safe human–robot interaction, it is important to design control schemes that ensure closed-loop stability and the generation of bounded control actions considering the saturation effect of actuators.

In order to solve this problem, various control structures with bounded actions have been proposed, such as output feedback proportional–integral–derivative (PID)-type schemes for global position stabilization, saturating PD+ control schemes for trajectory tracking, saturating PD-type controllers, among others [5–7]. These control schemes have been efficiently used for unconstrained motion tasks; nevertheless, most of the robotic systems used in medicine are in direct contact with a patient [8–10]; therefore, constrained motion control techniques are required to regulate human–robot interaction.

One of the main techniques to regulate the constrained motion of robot manipulators is impedance control. This methodology relates position and velocity errors to contact forces to generate adequate interaction dynamics by changing the mechanical impedance of the manipulator and

✉ Marco O. Mendoza-Gutiérrez
marco.mendoza@uaslp.mx

Victor I. Ramírez-Vera
a190243@alumnos.uaslp.mx

Isela Bonilla-Gutiérrez
isela.bonilla@uaslp.mx

[1] Faculty of Sciences, Autonomous University of San Luis Potosí, Av. Chapultepec 1570, Privadas del Pedregal, 78295 San Luis Potosí, SLP, Mexico

its environment [11]. Recently, some advanced impedance-based schemes such as hybrid position/impedance control, variable impedance control for physical human–robot interaction, or inverse reinforcement learning controllers have been proposed [12–14]. Similarly, various adaptive impedance control schemes have been proposed for interaction tasks where there is parametric uncertainty [15], such as reinforcement learning control [16], visual guidance control [17], discontinuous force-based control [18], iterative control and kinesthetic teaching [19], and finite-time control [20,21]. However, despite its adequate performance, these schemes do not address the actuator saturation effect and some omit the stability analysis or do not guarantee global closed-loop stability. Other proposals such as [22–24] avoid actuator saturation and consider bounded velocity and acceleration, respectively; however, the structure of such control schemes does not guarantee the generation of directly bounded actions, but rather limits the range of selection of control gains to achieve it, and this may compromise or limit the correct performance of the system. Early interaction control approaches that ensure the generation of bounded actions have made use of generalized saturation functions but have focused on addressing the problem of regulation (position control) through stiffness control [25,26], while our proposal addresses the tracking or motion control (position and velocity control) in constrained space by using impedance control.

Most of the force/impedance control schemes are task-space (Cartesian) controllers and use force/torque sensors to estimate external forces and torques due to the robot–environment interaction; nevertheless, this entails a mapping from joint space to Cartesian space and may cause singularities. In order to work in joint space and avoid singularities in human–robot interaction tasks, we can employ the electromyographic signal (EMG) to reflect the user's muscle activation and movement intention [27]. This signal has been effectively used in impedance control schemes as in [28] where the EMG is employed to estimate impedance parameters and a force/torque sensor is needed for calibration purposes, while in [29] the EMG is used to estimate human force, but a force sensor is also used to train an artificial neural network. Recently, in [30] the authors proposed a sensor-less impedance controller by using extended Kalman filters; however, these EMG-based controllers do not allow the generation of bounded control actions.

As far as we know, and from the literature review carried out, control schemes proposed for human–robot interaction tasks do not consider the physical limits of the actuators and a stability analysis is seldom included. Most controllers work in Cartesian space, so they are sensitive to singularities and require force/torque sensors or estimators that measure user intent in a more natural way. To overcome these limitations, we present a joint-space impedance controller with bounded actions that makes use of EMG to estimate the user's joint torque during human–robot interaction. It should be noted that the proposed scheme combines the main features of the schemes presented in [7,31,32], including a nonlinear PD+ structure based on generalized saturation functions for impedance control and external torque compensation based on EMG and the Hill muscle model. The correct performance of the proposed control scheme is supported by a stability analysis in the Lyapunov sense and numerical simulation results in human–robot interaction tasks.

2 Preliminaries

2.1 Notation and Definitions

Let $A \in \mathbb{R}^{n\times m}$ and $y \in \mathbb{R}^n$, while A_i is the ith row vector of matrix A, A_{ij} is the element of matrix A located in the ith row and the jth column, and y_i represents the ith element of vector y. The origin of $\mathbb{R}^n$ is denoted by 0_n, and the $n \times n$ identity matrix is represented as I_n. The Euclidean norm of vectors and the induced norm of matrices are denoted by $\|y\| = y^T y$ and $\|A\| = \lambda_{\max}\{A^T A\}$, respectively, where $\lambda_{\max}\{A^T A\}$ is the maximum eigenvalue of matrix $A^T A$.

Let $\mathcal{C}^k(\cdot)$ be the set of k-times continuously differentiable functions. Now, let $\zeta : \mathbb{R} \longmapsto \mathbb{R}$ be a continuously differentiable scalar function and $\varphi : \mathbb{R} \longmapsto \mathbb{R}$ be a locally Lipschitz, continuous, scalar function, both vanishing at zero, i.e., $\zeta(0) = \varphi(0) = 0$. In addition, ζ' represents the derivative of ζ with respect to its argument, i.e., $\zeta'(\varsigma) = \partial\zeta(\varsigma)/\partial\varsigma$. While the upper right-hand derivative of φ is given by $D^+\varphi(\varsigma) = \limsup_{h\to 0^+}[\varphi(\varsigma + h) - \varphi(\varsigma)]/h$, $\forall \varsigma \in \mathbb{R}$, thus $\varphi(\varsigma) = \int_0^{\varsigma} D^+\varphi(r)\,\mathrm{d}r$ [33].

Definition 1 A nondecreasing Lipschitz continuous function $\sigma : \mathbb{R} \to \mathbb{R}$ bounded by $M > 0$ is a generalized saturation function (GSF) if

(a) $\varsigma\sigma(\varsigma) > 0, \forall \varsigma \neq 0$.
(b) $|\sigma(\varsigma)| \leq M, \forall \varsigma \in \mathbb{R}$.
(c) In addition, if $\sigma(\varsigma) = \varsigma$ when $|\varsigma| \leq L$, for some $0 < L \leq M$, then σ is a linear generalized saturation function (L-GSF) for (L, M).

Furthermore, the function σ satisfies the following properties for a constant $k > 0$ [34,35]:

1. $\lim_{|\varsigma|\to\infty} D^+\sigma(\varsigma) = 0$.
2. $\exists \sigma'_M \in (0, \infty) : 0 \leq D^+\sigma(\varsigma) \leq \sigma'_M, \forall \varsigma \in \mathbb{R}$.
3. $\frac{\sigma^2(k\varsigma)}{2k\sigma'_M} \leq \int_0^{\varsigma} \sigma(kr)\mathrm{d}r \leq \frac{k\sigma'_M\varsigma^2}{2}, \forall \varsigma \in \mathbb{R}$.
4. $\int_0^{\varsigma} \sigma(kr)\mathrm{d}r > 0, \forall \varsigma \neq 0$.
5. $\int_0^{\varsigma} \sigma(kr)\mathrm{d}r \to \infty$ as $\varsigma \to \infty$.
6. If σ is strictly increasing, then

a. $\varsigma[\sigma(\varsigma+\eta)-\sigma(\eta)]>0, \forall \varsigma \neq 0, \forall \eta \in \mathbb{R}$.
b. $\bar{\sigma}(\varsigma)=\sigma(\varsigma+a)-\sigma(a)$ is a strictly increasing generalized saturation function (SI-GSF), for any constant $a \in \mathbb{R}$ and bounded by $\bar{M}=M+|\sigma(a)|$.

7. If σ is a linear saturation for (L, M), then, for any continuous function $\nu: \mathbb{R} \mapsto \mathbb{R}$ such that $|\nu(\eta)|<L, \forall \eta \in \mathbb{R}$, it holds that $\varsigma[\sigma(\varsigma+\nu(\eta))-\sigma(\nu(\eta))]>0, \forall \varsigma \neq 0, \forall \eta \in \mathbb{R}$.

2.2 Dynamic Model of Robot Manipulators

The Euler–Lagrange dynamical equation in joint space for robot manipulators, with n degrees of freedom, is given by

$$H(q)\ddot{q}+C(q,\dot{q})\dot{q}+F\dot{q}+g(q)=\tau-\tau_e \tag{1}$$

where $q \in \mathbb{R}^n$, $\dot{q} \in \mathbb{R}^n$, and $\ddot{q} \in \mathbb{R}^n$ are the joint position, velocity, and acceleration vectors, respectively. $H(q) \in \mathbb{R}^{n\times n}$, $C(q,\dot{q}) \in \mathbb{R}^{n\times n}$, and $F \in \mathbb{R}^{n\times n}$ are matrices of inertia, centripetal, and Coriolis and viscous friction torques, respectively. Finally, $g(q) \in \mathbb{R}^n$, $\tau \in \mathbb{R}^n$ and $\tau_e \in \mathbb{R}^m$ are vectors of gravitational, control, and external interaction torques, respectively.

The following properties of the dynamic model (1) are useful for further analysis [36].

Property 1 $H(q)$ and F are positive definite symmetric matrices, even F is diagonal.

Property 2 For some constants $\mu_M \geq \mu_m > 0$, $H(q)$ satisfies $\mu_m I_n \leq H(q) \leq \mu_M I_n, \forall q \in \mathbb{R}^n$.

Property 3 For robots with only revolute joints, $H(q)$ is bounded on $\mathbb{R}^{n\times n}$ in such a way that $\|H_i(q)\| \leq \mu_{Mi}$, $\forall q \in \mathbb{R}^n$ and nonnegative constants $\mu_{Mi}, i=1,\ldots,n$.

Property 4 $C(q,\dot{q})$ and $\dot{H}(q,\dot{q}) \triangleq \frac{dH(q)}{dt}$ satisfy $\dot{q}^T\left[\dot{H}(q,\dot{q})-2C(q,\dot{q})\right]\dot{q}=0$ and actually $\dot{H}(q,\dot{q})=C(q,\dot{q})+C^T(q,\dot{q}), \forall (q,\dot{q}) \in \mathbb{R}^n \times \mathbb{R}^n$.

Property 5 The matrix $C(q,\dot{q})$ satisfies $C(w,x+y)z=C(w,x)z+C(w,y)z$ and $C(x,y)z=C(x,z)y, \forall w,x,y,z \in \mathbb{R}^n$.

Property 6 For some constant $k_c \geq 0$, $C(q,\dot{q})$ satisfies $\|C(x,y)z\| \leq k_c\|y\|\|z\|$, $\forall x,y,z \in \mathbb{R}^n$. In addition, there are nonnegative constants k_{ci} such that $|C_i(x,y)z| \leq k_{ci}\|y\|\|z\|, i=1,\ldots,n, \forall x,y,z \in \mathbb{R}^n$

Property 7 For some constants $f_M \geq f_m > 0$, F satisfies $f_m\|x\|^2 \leq x^T F x \leq f_M\|x\|^2, \forall x \in \mathbb{R}^n$. In addition, as F is a diagonal matrix, there are nonnegative constants f_{Mi} such that $|F_i x| \leq f_{Mi}\|x\|, i=1,\ldots,n, \forall x \in \mathbb{R}^n$.

Property 8 For robots with only revolute joints, $g(q)$ is bounded on $\mathbb{R}^n$ in such a way that $|g_i(q)| \leq B_{gi}, \forall q \in \mathbb{R}^n$ and nonnegative constants $B_{gi}, i=1,\ldots,n$.

Property 9 The left-hand side of the dynamic model (1) is linear with respect to its parameters; therefore, it can be rewritten as

$$H(q,\theta)\ddot{q}+C(q,\dot{q},\theta)\dot{q}+F(\theta)\dot{q}+g(q,\theta)=Y(q,\dot{q},\ddot{q})\theta \tag{2}$$

where $Y(q,\dot{q},\ddot{q}) \in \mathbb{R}^{n\times p}$ is a regression matrix and $\theta \in \mathbb{R}^p$ is a constant vector of robot parameters. Now, let $\theta_{Ml} > 0$ be an upper bound of $|\theta_l|$, i.e., $|\theta_l| \leq \theta_{Ml}$ $\forall l \in \{1,...,p\}$, $\theta_M \triangleq (\theta_{M1},...,\theta_{Mp})^T$, and $\Theta \triangleq [-\theta_{M1},\theta_{M1}] \times \cdots \times [-\theta_{Mp},\theta_{Mp}]$, also let $\mathcal{X}$ and $\mathcal{Y}$ be compact subsets of $\mathbb{R}^n$; by Properties 2, 6, 7, and 8, there are constants $B_{Di} > 0$ such that $|Y_i(w,x,y)z| \leq B_{Di}$, $\forall w \in \mathbb{R}^n$, $(x,y) \in \mathcal{X} \times \mathcal{Y}$ and $\forall z \in \Theta$.

Assumption 1 For robots with bounded inputs, each element of vector τ is bounded by $T_i > 0$, i.e., $|\tau_i| \leq T_i, i=1,\ldots,n$. Assume that

$$\tau_i = T_i \text{sat}\left(\frac{u_i}{T_i}\right) \tag{3}$$

where $\text{sat}(\cdot)$ is the standard saturation function, i.e., $\text{sat}(\varsigma)=\text{sign}(\varsigma)\min\{|\varsigma|,1\}$ and u_i denotes the ith control signal.

2.3 External Interaction Torque Model

In order to model the torques generated by human–robot interaction, the Hill-type muscle model is considered. Hill's model allows us to relate the muscle activity represented by the electromyographic signal (EMG) to the muscle forces/torques generated in a certain joint.

The EMG must be processed and conditioned before use within Hill's model. First, the signal amplitude (aEMG) must be obtained and at least the following elements are required: a) high-pass filter with cutoff frequency between 10 and 30 Hz, b) rectifier, and c) low-pass filter with cutoff frequency between 2 and 10 Hz. Next, the maximum voluntary contraction (MVC) of the user must be obtained and the aEMG using the MVC value is normalized [32].

Assume that m muscles are involved in the generation of the ith joint torque, then the aEMG of each of these muscles (a_{EMGj}) is used to obtain the muscle activation given by

$$a_j(t)=\frac{e^{k_{Aj}a_{EMGj}(t)}-1}{e^{k_{Aj}}-1} \tag{4}$$

where $j \in \{1,...,m\}$, $-3 \leq k_A < 0$ represents the nonlinearity between neuronal and muscular activation. According

to Hill's model, the muscle–tendon force is obtained as

$$f_{MTj} = [f_{MAj} + f_{MPj}] \cos\theta_j \tag{5}$$

where θ_j is the pennation angle of jth muscle fibers and

$$f_{MAj} = f_{Aj} f_{Vj} f_{M0j} a_j(t) \tag{6}$$
$$f_{MPj} = f_{Pj} f_{M0j} \tag{7}$$

are the components of active and passive muscle force, respectively, with f_{M0j} being the jth maximum (optimal) isometric force and, according to [32],

$$f_{Aj} = \begin{cases} h_{0j} + h_{1j} l_j + h_{2j} l_j^2, & \text{for } 0.5 < l_j \leq 1.5 \\ 0, & \text{otherwise} \end{cases} \tag{8}$$
$$f_{Vj} = 1 \tag{9}$$
$$f_{Pj} = \mathrm{e}^{10 l_j - 15} \tag{10}$$

where l_j represents the jth normalized muscle length and h_{0j}, h_{1j}, and h_{2j} are constant parameters that are chosen according to the force–length curve adjustment algorithm [37].

Finally, the joint torque is given by

$$u_{ei} = \sum_{j=1}^{m} f_{MTj} r_j \tag{11}$$

where $i \in \{1, ..., n\}$ and r_j is the moment arm of jth muscle.

Assumption 2 The muscle torques are bounded and can be modeled using GSFs in such a way that

$$\tau_{ei} = \sigma_{e_i}(u_{ei}) \tag{12}$$

where σ_{ei} are linear SI-GSFs bounded by (L_{ei}, M_{ei}), $\forall i \in \{1, ..., n\}$.

3 Impedance Control with Bounded Actions

3.1 Definition of the Control Problem

The impedance control approach presented in this paper corresponds to a generalization of motion control in joint space by choosing a desired trajectory $q_d(t) \in \mathbb{R}^n$ while respecting the following dynamic relationship:

$$q - q_d = \mathcal{F}(s)\tau_e \tag{13}$$

where

$$\mathcal{F}(s) = [H_E s^2 + D_E s + K_E]^{-1} \tag{14}$$

with $H_E = \mathrm{diag}[h_{E1}, ..., h_{En}]$, $D_E = \mathrm{diag}[d_{E1}, ..., d_{En}]$, and $K_E = \mathrm{diag}[k_{E1}, ..., k_{En}]$ being positive definite matrices of inertia, damping, and stiffness, respectively, and s representing the Laplace complex variable. Then, the impedance error in joint space can be defined as

$$\bar{\xi} \triangleq \bar{q} - q_e \tag{15}$$

where $\bar{q} = q - q_d \in \mathbb{R}^n$ is the position error and $q_e = \mathcal{F}(s)\tau_e$ represents an adjustment to the position or path to follow due to robot–environment interaction.

Assumption 3 The reference trajectory to be tracked q_d belongs to $Q_d \triangleq \{q_d \in \mathcal{C}^2(\mathbb{R}_+; \mathbb{R}^n) : \|\dot{q}_d(t)\| \leq B_{dv}, \|\ddot{q}_d(t)\| \leq B_{da}, \forall t \geq 0\}$

Assumption 4 The vector q_e and its time derivatives $\dot{q}_e$ and $\ddot{q}_e$ are bounded; then, there are nonnegative constants such that $|q_{ei}| \leq B_{epi}$, $\|q_e\| \leq B_{ep}$, $|\dot{q}_{ei}| \leq B_{evi}$, $\|\dot{q}_e\| \leq B_{ev}$, $|\ddot{q}_{ei}| \leq B_{eai}$ and $\|\ddot{q}_e\| \leq B_{ea}$, respectively, and satisfying that

$$k_{Ei} \geq M_{ei}/B_{epi} \tag{16}$$
$$h_{Ei} \geq B_{eai}/B_{evi} \tag{17}$$
$$d_{Ei} \geq 1.25 k_{Ei} h_{Ei} \tag{18}$$

The control problem addressed in this paper is to achieve an adequate robot–environment interaction while tracking a time-varying trajectory without exceeding the maximum torque limits of robot actuators. Therefore, the goal of our impedance control approach consists of designing u in such a way that

$$\lim_{t \to \infty} \bar{\xi} = 0 \tag{19}$$
$$\tau_i < T_i \tag{20}$$

$\forall t \geq 0, i = 1, ..., n.$

3.2 Saturating Impedance Controller

In order to control the robot–environment interaction while respecting the saturation limits of the robotic system and operating directly in the joint space to avoid singularities, the following impedance control scheme is proposed:

$$u = -s_P(K_P \bar{\xi}) - s_D(K_D \dot{\bar{\xi}}) + Y(q, \dot{q}_h, \ddot{q}_h)\theta + \tau_e \tag{21}$$

where, according to Property 9,

$$Y(q, \dot{q}_h, \ddot{q}_h)\theta = H(q, \theta)\ddot{q}_h + C(q, \dot{q}_h, \theta)\dot{q}_h + F(\theta)\dot{q}_h + g(q, \theta) \tag{22}$$

with $\dot{q}_h = \dot{q}_d + \dot{q}_e$ and $\ddot{q}_h = \ddot{q}_d + \ddot{q}_e$; $K_P = \text{diag}[k_{P1}, ..., k_{Pn}]$; and $K_D = \text{diag}[k_{D1}, ..., k_{Dn}]$ being positive definite matrices of proportional and derivative gains, respectively, while $s_P(x) = (\sigma_{P1}(x_1), ..., \sigma_{Pn}(x_n))^T$ and $s_D(x) = (\sigma_{D1}(x_1), ..., \sigma_{Dn}(x_n))^T$ with $\sigma_{Pi}(\cdot)$ and $\sigma_{Di}(\cdot)$ being continuously differentiable GSFs bounded by M_{Pi} and M_{Di}, respectively. In addition,

$$\left\| s_D(K_D \dot{\bar{\xi}}) \right\| \leq \kappa \left\| \dot{\bar{\xi}} \right\| \tag{23}$$

where $\kappa = \max_i \{\sigma'_{DiM} k_{Di}\}$.

In addition, according to Property 9 and Assumptions 1–4, and considering a robot manipulator with actuators to ensure that $|Y_i(q, \dot{q}_h, \ddot{q}_h)\theta + \tau_{ei}| < T_i$, the controller (21)–(22) produces bounded actions if M_{Pi} and M_{Di} satisfy

$$M_{Pi} + M_{Di} < T_i - B_{Di} - M_{ei} \tag{24}$$

$\forall i = 1, ..., n$, where

$$B_{Di} = \mu_{Mi} B_{ha} + k_{ci} B_{hv}^2 + f_{Mi} B_{hv} + B_{gi} \tag{25}$$

with $B_{ha} = B_{da} + B_{ea}$ and $B_{hv} = B_{dv} + B_{ev}$.

3.3 Closed-Loop Analysis

By combining the robot model (1), the environment model (12), and the control scheme (21)–(22), the closed-loop dynamics (with abuse of notation) can be represented as

$$\frac{d}{dt}\begin{bmatrix} \bar{\xi} \\ \dot{\bar{\xi}} \end{bmatrix} = \begin{bmatrix} \dot{\bar{\xi}} \\ H^{-1}(q)\left\{ -s_P(K_P\bar{\xi}) - s_D(K_D\dot{\bar{\xi}}) - [C(q,\dot{q}) + C(q,\dot{q}_h)]\dot{\bar{\xi}} - F\dot{\bar{\xi}} \right\} \end{bmatrix} \tag{26}$$

where Property 5 has been considered. Now, under stationary conditions $\dot{\bar{\xi}} = \ddot{\bar{\xi}} = 0_n$ we obtain that

$$-s_P\left(K_P\bar{\xi}\right) = 0_n \tag{27}$$

Then, $\bar{\xi} = \dot{\bar{\xi}} = 0_n$ is the unique equilibrium vector.

3.4 Lyapunov Stability Analysis

In order to analyze the stability of closed-loop equilibrium vector, consider the following scalar candidate function:

$$V(t, \bar{\xi}, \dot{\bar{\xi}}) = \frac{1}{2}\dot{\bar{\xi}}^T H(q)\dot{\bar{\xi}} + \int_{0_n}^{\bar{\xi}} s_P^T (K_P r)\, \mathrm{d}r + \epsilon \dot{\bar{\xi}}^T H(q) s_P\left(K_P\bar{\xi}\right) \tag{28}$$

where $\int_{0_n}^{\bar{\xi}} s_P^T (K_P r)\, \mathrm{d}r = \sum_{i=1}^n \int_0^{\bar{\xi}_i} \sigma_{Pi}(k_{Pi} r_i)\, \mathrm{d}r_i$. To demonstrate that this candidate function is positive definite and decreasing, the function (28) is rewritten as

$$V(t, \bar{\xi}, \dot{\bar{\xi}}) = V_0(t, \bar{\xi}, \dot{\bar{\xi}}) + (1-\alpha)\int_{0_n}^{\bar{\xi}} s_P^T (K_P r)\, \mathrm{d}r \tag{29}$$

where

$$V_0(t, \bar{\xi}, \dot{\bar{\xi}}) = \frac{1}{2}\dot{\bar{\xi}}^T H(q)\dot{\bar{\xi}} + \alpha \int_{0_n}^{\bar{\xi}} s_P^T (K_P r)\, \mathrm{d}r + \epsilon \dot{\bar{\xi}}^T H(q) s_P\left(K_P\bar{\xi}\right) \tag{30}$$

with $0 < \alpha < 1$. Then, according to Definition 1 and Property 2, $V_0(t, \bar{\xi}, \dot{\bar{\xi}})$ is lower-bounded by

$$\begin{aligned} W_0(\bar{\xi}, \dot{\bar{\xi}}) &= \frac{1}{2}\mu_m \|\dot{\bar{\xi}}\|^2 + \frac{\alpha}{2\beta_P}\|s_P\left(K_P\bar{\xi}\right)\|^2 - \epsilon\mu_M \|s_P\left(K_P\bar{\xi}\right)\| \|\dot{\bar{\xi}}\| \\ &= \frac{1}{2}\begin{bmatrix} \|s_P\left(K_P\bar{\xi}\right)\| \\ \|\dot{\bar{\xi}}\| \end{bmatrix}^T \begin{bmatrix} \alpha/\beta_P & -\epsilon\mu_M \\ -\epsilon\mu_M & \mu_m \end{bmatrix} \times \begin{bmatrix} \|s_P\left(K_P\bar{\xi}\right)\| \\ \|\dot{\bar{\xi}}\| \end{bmatrix} \end{aligned} \tag{31}$$

where $\beta_P = \max_i \{\sigma'_{PiM} k_{Pi}\}$ and with

$$1 > \alpha > \frac{\epsilon^2}{\epsilon_1^2} \tag{32}$$

$$\epsilon_1 = \sqrt{\frac{\mu_m}{\mu_M^2 \beta_P}} \tag{33}$$

if $\epsilon < \epsilon_1$, $W_0(\bar{\xi}, \dot{\bar{\xi}})$ is positive definite. Also, note that $W_0(0_n, \dot{\bar{\xi}}) \to \infty$ as $\|\dot{\bar{\xi}}\| \to \infty$.

On the other hand, $V(t, \bar{\xi}, \dot{\bar{\xi}})$ is upper-bounded by

$$\begin{aligned} W_1(\bar{\xi}, \dot{\bar{\xi}}) &= \frac{1}{2}\mu_M \|\dot{\bar{\xi}}\|^2 + \beta_P \|\bar{\xi}\|^2 + \epsilon\mu_M\beta_P \|\bar{\xi}\| \|\dot{\bar{\xi}}\| \\ &= \frac{1}{2}\begin{bmatrix} \|\bar{\xi}\| \\ \|\dot{\bar{\xi}}\| \end{bmatrix}^T \begin{bmatrix} \beta_P & \epsilon\mu_M\beta_P \\ \epsilon\mu_M\beta_P & \mu_M \end{bmatrix} \begin{bmatrix} \|\bar{\xi}\| \\ \|\dot{\bar{\xi}}\| \end{bmatrix} \end{aligned} \tag{34}$$

where again Definition 1 and Property 2 have been used. Now, $W_1(\bar{\xi}, \dot{\bar{\xi}})$ is positive definite if

$$\epsilon^2 < \frac{1}{\mu_M \beta_P} \tag{35}$$

and as $\mu_M > \mu_m$, then it is enough that again $\epsilon < \epsilon_1$.

Therefore,

$$W_1(\bar{\xi}, \dot{\bar{\xi}}) \geq V(t, \bar{\xi}, \dot{\bar{\xi}}) \geq W_0(\bar{\xi}, \dot{\bar{\xi}}) + (1-\alpha) \int_{0_n}^{\bar{\xi}} s_P^T (K_P r)\, \mathrm{d}r \tag{36}$$

and we can conclude that $V(t, \bar{\xi}, \dot{\bar{\xi}})$ is a radially unbounded positive definite and decreasing function.

Now, the upper right-hand derivative of (28) along the trajectories of the closed-loop system (26) is

$$\begin{aligned}
\dot{V}(t, \bar{\xi}, \dot{\bar{\xi}}) = {} & \dot{\bar{\xi}}^T H(q) \ddot{\bar{\xi}} + \frac{1}{2} \dot{\bar{\xi}}^T \dot{H}(q, \dot{q}) \dot{\bar{\xi}} \\
& + s_P^T(K_P \bar{\xi}) \dot{\bar{\xi}} + \epsilon s_P^T(K_P \bar{\xi}) H(q) \ddot{\bar{\xi}} \\
& + \epsilon \dot{\bar{\xi}}^T \dot{H}(q, \dot{q}) s_P(K_P \bar{\xi}) \\
& + \epsilon \dot{\bar{\xi}}^T H(q) s_P'(K_P \bar{\xi}) K_P \dot{\bar{\xi}} \\
= {} & \dot{\bar{\xi}}^T \Big\{ -s_P(K_P \bar{\xi}) - s_D(K_D \dot{\bar{\xi}}) \\
& - [C(q, \dot{q}) + C(q, \dot{q}_h)] \dot{\bar{\xi}} - F \dot{\bar{\xi}} \Big\} \\
& + \frac{1}{2} \dot{\bar{\xi}}^T \dot{H}(q, \dot{q}) \dot{\bar{\xi}} + s_P^T(K_P \bar{\xi}) \dot{\bar{\xi}} \\
& + \epsilon \dot{\bar{\xi}}^T \dot{H}(q, \dot{q}) s_P(K_P \bar{\xi}) + \epsilon s_P^T(K_P \bar{\xi}) \\
& \times \Big\{ -s_P(K_P \bar{\xi}) - s_D(K_D \dot{\bar{\xi}}) \\
& - [C(q, \dot{q}) + C(q, \dot{q}_h)] \dot{\bar{\xi}} - F \dot{\bar{\xi}} \Big\} \\
& + \epsilon \dot{\bar{\xi}}^T H(q) s_P'(K_P \bar{\xi}) K_P \dot{\bar{\xi}} \\
= {} & -\dot{\bar{\xi}}^T s_D(K_D \dot{\bar{\xi}}) - \dot{\bar{\xi}}^T C(q, \dot{q}_h) \dot{\bar{\xi}} \\
& - \dot{\bar{\xi}}^T F \dot{\bar{\xi}} - \epsilon s_P^T(K_P \bar{\xi}) s_P(K_P \bar{\xi}) \\
& - \epsilon s_P^T(K_P \bar{\xi}) s_D(K_D \dot{\bar{\xi}}) \\
& - \epsilon \dot{\bar{\xi}}^T [C(q, \dot{\bar{\xi}}) + C(q, \dot{q}_h)] s_P(K_P \bar{\xi}) \\
& - \epsilon s_P^T(K_P \bar{\xi}) F \dot{\bar{\xi}} - \epsilon s_P^T(K_P \bar{\xi}) C(q, \dot{q}_h) \dot{\bar{\xi}} \\
& + \epsilon \dot{\bar{\xi}}^T H(q) s_P'(K_P \bar{\xi}) K_P \dot{\bar{\xi}}
\end{aligned} \tag{37}$$

where Property 4 was used. Then, by employing Properties 2, 5, 6, 7, and 8, Assumptions 3 and 4, and inequality (23), $\dot{V}(t, \bar{\xi}, \dot{\bar{\xi}})$ can be upper-bounded as

$$\dot{V}(t, \bar{\xi}, \dot{\bar{\xi}}) \leq -\dot{\bar{\xi}}^T s_D(K_D \dot{\bar{\xi}}) - W_2(\bar{\xi}, \dot{\bar{\xi}}) \tag{38}$$

where

$$\begin{aligned}
W_2(\bar{\xi}, \dot{\bar{\xi}}) = {} & -k_c B_{hv} \|\dot{\bar{\xi}}\|^2 + f_m \|\dot{\bar{\xi}}\|^2 + \epsilon \|s_P(K_P \bar{\xi})\|^2 \\
& - \epsilon \kappa \|s_P(K_P \bar{\xi})\| \|\dot{\bar{\xi}}\| - \epsilon k_c B_P \|\dot{\bar{\xi}}\|^2 \\
& - \epsilon k_c B_{hv} \|s_P(K_P \bar{\xi})\| \|\dot{\bar{\xi}}\| \\
& - \epsilon f_M \|s_P(K_P \bar{\xi})\| \|\dot{\bar{\xi}}\| \\
& - \epsilon k_c B_{hv} \|s_P(K_P \bar{\xi})\| \|\dot{\bar{\xi}}\| - \epsilon \mu_M \beta_P \|\dot{\bar{\xi}}\|^2 \\
= {} & \begin{bmatrix} \|s_P\left(K_P \bar{\xi}\right)\| \\ \|\dot{\bar{\xi}}\| \end{bmatrix}^T Q_2 \begin{bmatrix} \|s_P\left(K_P \bar{\xi}\right)\| \\ \|\dot{\bar{\xi}}\| \end{bmatrix}
\end{aligned} \tag{39}$$

with $B_P = \sqrt{\sum_{i=1}^{n} M_{Pi}^2}$ and

$$Q_2 = \begin{bmatrix} \epsilon & -\epsilon\left(\frac{\kappa + f_M}{2} + k_c B_{hv}\right) \\ -\epsilon\left(\frac{\kappa + f_M}{2} + k_c B_{hv}\right) & f_m - k_c B_{hv} - \epsilon(k_c B_P + \mu_M \beta_P) \end{bmatrix} \tag{40}$$

which is positive definite if $\epsilon < \epsilon_2$ for

$$\epsilon_2 = \frac{f_m - k_c B_{hv}}{k_c B_P + \mu_M \beta_P + \left(\frac{\kappa + f_M}{2} + k_c B_{hv}\right)^2}, \tag{41}$$

then, $B_{hv} < f_m / k_c$. Thus, by satisfying $\epsilon < \min\{\epsilon_1, \epsilon_2\}$, we can conclude that $\dot{V}(t, \bar{\xi}, \dot{\bar{\xi}}) < 0$ and the equilibrium point of closed-loop (non-autonomous) system (26) is globally uniformly asymptotically stable.

4 Numerical Simulation

The validation of the proposed control scheme was carried out by one numerical simulation test of a human–robot interaction task, where a comparative analysis of the performance of our scheme and two controllers with a similar structure was conducted. The interaction task implemented assumes that the robotic system is coupled externally to a person's arm (simulating an exoskeleton) and the elbow rotation axes of both are coincident. Initially, the robot has a predefined desired trajectory and will have to adapt or modify its movement depending on the active participation of the person, i.e., when the torque applied by the user is greater than zero.

For the implementation of controllers with bounded actions, the following generalized saturation functions were used:

$$\sigma_h(\varsigma; M) = M \mathrm{sat}(\varsigma / M) \tag{42}$$

$$\sigma_s(\varsigma; L, M) = \begin{cases} \varsigma, & \forall |\varsigma| \leq L \\ \rho_s(\varsigma), & \forall |\varsigma| > L \end{cases} \tag{43}$$

where

$$\rho_s(\varsigma) = \text{sign}(\varsigma)L + (M - L)\tanh\left(\frac{\varsigma - \text{sign}(\varsigma)L}{M - L}\right) \quad (44)$$

4.1 Model of the Robotic Platform

The robotic platform used in simulation tests corresponds to a two-degree-of-freedom robot manipulator whose modeling and dynamic parameterization were presented in [38]. The robot actuators have as torque limit values $T_1 = 200$ Nm and $T_2 = 15$ Nm, respectively, while the corresponding positive constants that satisfy Properties 2, 6, 7, and 8 are: $\mu_m = 0.088\ \text{kg·m}^2$, $\mu_M = 2.533\ \text{kg·m}^2$, $\mu_{M1} = 2.526\ \text{kg·m}^2$, $\mu_{M2} = 0.213\ \text{kg·m}^2$, $k_c = 0.146\ \text{kg·m}^2$, $k_{c1} = 0.136\ \text{kg·m}^2$, $k_{c2} = 0.084\ \text{kg·m}^2$, $f_m = f_{M2} = 0.175\ \text{kg·m}^2/\text{s}$, $f_M = f_{M1} = 2.288\ \text{kg·m}^2/\text{s}$, $B_{g1} = 40.29$ Nm, and $B_{g2} = 1.825$ Nm, respectively. Besides, for this robot, we have that

$$Y(q, \dot{q}, \ddot{q}) = \begin{bmatrix} \ddot{q}_1 & 0 \\ (2\ddot{q}_1 + \ddot{q}_2)c_2 - \dot{q}_2(2\dot{q}_1 + \dot{q}_2)s_2 & \ddot{q}_1 c_2 + \dot{q}_1^2 s_2 \\ \ddot{q}_2 & \ddot{q}_1 + \ddot{q}_2 \\ \dot{q}_1 & 0 \\ 0 & \dot{q}_2 \\ \sin q_1 & 0 \\ \sin(q_1 + q_2) & \sin(q_1 + q_2) \end{bmatrix} \quad (45)$$

$$\theta = \begin{bmatrix} 2.351 & 0.084 & 0.102 & 2.288 & 0.175 & 38.465 & 1.825 \end{bmatrix}^T \quad (46)$$

to satisfy Property 9 and where $c_2 = \cos q_2$ and $s_2 = \sin q_2$.

4.2 Model of Human-Applied Torques

In order to simulate the torques applied by a human interacting with the robot, EMG signals of biceps and triceps muscles from the database [39] were used as inputs to the model described in Sect. 2.3. First, the EMG signals were preprocessed using the cutoff frequency of 10 Hz for high-pass and 400 Hz for low-pass filters. According to the database, the MVC values for the biceps and triceps are 7527.5 and 1776.6, respectively. Therefore, it was only considered that there is an external torque applied to the elbow joint and the shoulder joint moves freely, i.e., $\tau_{e1} = 0$ Nm ($M_{e1} = 0$).

The values selected for the constants of the Hill model (4)–(11) were: $k_{A1} = k_{A2} = -2$, $\theta_1 = 0^o$, $\theta_2 = 10^o$, $f_{M01} = 400$ Nm, $f_{M02} = 600$ Nm, $h_{01} = h_{02} = -2.06$, $h_{11} = h_{12} = 6.16$, $h_{21} = h_{22} = -3.13$, $l_1 = l_2 = 0.8$, $r_1 = 0.0153$ m, and $r_2 = 0.01$ m, where sub-index 1 refers to biceps and sub-index 2 to triceps. In addition, to model the bounded behavior of the interaction torque it was considered that

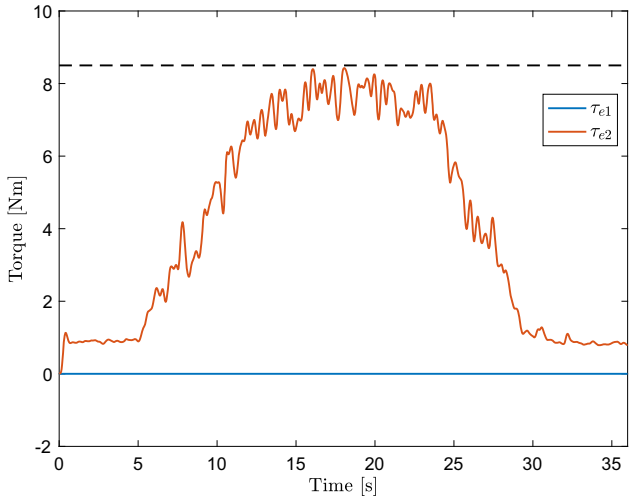

Fig. 1 Muscle torques obtained by the Hill model from EMG signals. The segmented line represents the bound $M_{e2} = 8.5$

$$\sigma_{e2}(\varsigma) = \sigma_s(\varsigma; L_{e2}, M_{e2}) \quad (47)$$

with $M_{e2} = 8.5$ and $L_{e2} = 0.9M_{e2}$ satisfying (12). The muscle torques obtained are shown in Fig. 1.

4.3 Configuration of the Impedance Controller

The trajectories to be followed by the robot's joints were chosen as

$$q_{d1}(t) = \frac{\pi}{2} + \sin \omega t \quad (48)$$

$$q_{d2}(t) = \cos \omega t \quad (49)$$

where, according to Assumptions 3 and 4, $\omega = B_{dv} < f_m/k_c - B_{ev}$. Then, $B_{da} = \omega^2$ and we can select $B_{ep} = 0.85$, $B_{ev} = 0.15$, $B_{ea} = 0.3$ obtaining that $\omega < 1.049$ rad/s. Therefore, we set $\omega = 1$ rad/s and the impedance parameters that characterize the dynamics of human–robot interaction were tuned as $k_{E2} = 10$, $h_{E2} = 2$, and $d_{E2} = 25$ to satisfy (16), (17), and (18), respectively.

The proportional and derivative actions of the impedance controller (21) were implemented with

$$\sigma_{Pi}(\varsigma) = \sigma_s(\varsigma; L_{Pi}, M_{Pi}) \quad (50)$$

$$\sigma_{Di}(\varsigma) = \sigma_h(\varsigma; M_{Di}) \quad (51)$$

$i = 1, 2$. Therefore, $\sigma'_{PiM} = \sigma'_{DiM} = 1$ and $\kappa = \max_i\{k_{Di}\}$. In order to obtain bounded control actions, $M_{P1} = M_{D1} = 40$, $L_{P1} = 0.9M_{P1}$, $M_{P2} = M_{D2} = 2$, and $L_{P2} = 0.9M_{P2}$ were chosen to satisfy (24) with $B_{D1} = 46.385$ and $B_{D2} = 2.414$ according to the values of the robot's dynamic parameters, while the dynamic compensation term $Y(q, \dot{q}_h, \ddot{q}_h)\theta$

was implemented by replacing $\dot{q}$ with $\dot{q}_h$ and $\ddot{q}$ with $\ddot{q}_h$ in (45). In addition, for the external torque compensation term τ_e, the estimated joint torque from the EMG signals described in Sect. 4.2 was used.

4.4 Results

For comparison purposes, the same human–robot interaction task was implemented using the adaptive controllers presented in [7,15], and to distinguish each of the controllers, the following nomenclature is used: JS-IC represents the joint-space impedance controller proposed in this paper, JS-TC is the joint-space tracking controller presented in [7], and TS-IC denotes the task-space impedance controller presented in [15]. The SP-SD+ adaptive tracking controller [7] is given by

$$u = -s_P(K_P\bar{q}) - s_D(K_D\dot{\bar{q}}) + Y(q,\dot{q}_d,\ddot{q}_d)\hat{\theta} \tag{52}$$

$$\dot{\phi} = -\Gamma Y^T(q,\dot{q}_d,\ddot{q}_d)[\dot{\bar{q}} + \varepsilon s_P(K_P\bar{q})] \tag{53}$$

$$\hat{\theta} = s_a(\phi) \tag{54}$$

where $\Gamma = \text{diag}[\gamma_1, ..., \gamma_p]$ is a (constant) positive definite matrix, while $s_a(x) = (\sigma_{a1}(x_1), ..., \sigma_{ap}(x_p))^T$ with $\sigma_{al}(\cdot)$ being strictly increasing GSFs bounded by $M_{al}, l = 1, ..., p$. The proportional and derivative actions were implemented as (50)–(51) with $M_{P1} = M_{D1} = 40$, $L_{P1} = 0.9M_{P1}$, $M_{P2} = M_{D2} = 4$, and $L_{P2} = 0.9M_{P2}$, while for the adaptive term

$$\sigma_{al}(\varsigma) = \sigma_s(\varsigma; L_{al}, M_{al}) \tag{55}$$

with $M_a = (2.939, 0.105, 0.127, 2.86, 0.219, 48.081, 2.281)^T$ and $L_{al} = 0.9M_{al}, l = 1, ..., 7$.

On the other hand, the adaptive impedance controller [15] is given by

$$\begin{aligned}\tau = {} & H_0(q,\hat{\theta}_d(0))J^{-1}(q,\hat{\theta}_k)[-K_P\bar{\xi} - K_D\hat{\zeta} - \dot{J}(q,\dot{q},\hat{\theta}_k)\\ & + C(q,\dot{q},\hat{\theta}_d)\dot{q} + g(q,\hat{\theta}_d)\\ & + J^T(q,\hat{\theta}_k)f_e + [H(q,\hat{\theta}_d) - H_0(q,\hat{\theta}_d(0))]\ddot{q}\end{aligned} \tag{56}$$

$$\dot{\hat{\theta}}_d = \Gamma_d J(q,\hat{\theta}_k)H_0^{-1}(q,\hat{\theta}_d(0))Y_d(q,\dot{q},\ddot{q})H_E[\dot{\bar{\xi}} + \hat{\zeta}] \tag{57}$$

$$\begin{aligned}\dot{\hat{\theta}}_k = {} & \Gamma_k[J(q,\hat{\theta}_k)H_0^{-1}(q,\hat{\theta}_d(0))Y_e(q,f_e)H_E[\dot{\bar{\xi}} + \hat{\zeta}]\\ & - W_k^T\Lambda_k(W_k\hat{\theta}_k - z)]\end{aligned} \tag{58}$$

where f_e is the task-space interaction force, $\bar{\xi} = x - x_d - x_e$ is the task-space impedance error, and $\hat{\zeta} = \dot{\hat{x}} - \dot{x}_d - \dot{x}_e$ is the estimate of $\dot{\bar{\xi}}$, with x being the Cartesian position of the robot's end effector (forward kinematics), x_d being the desired trajectory in Cartesian space (obtained by forward kinematics with q_d as input), and $x_e = \mathcal{F}(s)f_e$ being the trajectory adjustment vector in Cartesian space, whose parameters are $H_E = \text{diag}[2, 2]$, $D_E = \text{diag}[50, 50]$ and $K_E = \text{diag}[150, 150]$. $H_0(q,\hat{\theta}_d(0))$ is a symmetric and positive definite matrix that represents the initial estimate of $H(q)$, $\hat{\theta}_d$ and $\hat{\theta}_k$ are the estimated dynamic and kinematic parameter vectors, respectively, whose real values are

$$\theta_d = \begin{bmatrix}2.351 & 0.084 & 0.102 & 38.465 & 1.825\end{bmatrix}^T$$

$$\theta_k = \begin{bmatrix}0.45 & 0.45\end{bmatrix}^T,$$

while $J(q,\hat{\theta}_k)$ represents the estimate of analytical Jacobian matrix given by

$$J(q,\hat{\theta}_k) = \begin{bmatrix}\hat{\theta}_{k1}\cos q_1 + \hat{\theta}_{k2}\cos(q_1+q_2) & \hat{\theta}_{k2}\cos(q_1+q_2)\\ \hat{\theta}_{k1}\sin q_1 + \hat{\theta}_{k2}\sin(q_1+q_2) & \hat{\theta}_{k2}\sin(q_1+q_2)\end{bmatrix} \tag{59}$$

In addition, $\Gamma_d = \text{diag}[\gamma_{d1}, ..., \gamma_{d5}]$, $\Gamma_k = \text{diag}[\gamma_{k1}, \gamma_{k2}]$, and $\Lambda_k = \text{diag}[\lambda_{k1}, \lambda_{k2}]$ are (constant) positive definite matrices, $z = [\lambda s/(\lambda + s)]x$, $W_k = [\lambda/(\lambda + s)]Y_k(q,\dot{q})$ is a low-pass filter with $\lambda = 10$, and the corresponding regression matrices are

$$Y_k(q,\dot{q}) = \begin{bmatrix}\dot{q}_1\cos q_1 & [\dot{q}_1+\dot{q}_2]\cos(q_1+q_2)\\ \dot{q}_1\sin q_1 & [\dot{q}_1+\dot{q}_2]\sin(q_1+q_2)\end{bmatrix}$$

$$\begin{aligned}&Y_d(q,\dot{q},\ddot{q})\\ &= \begin{bmatrix}\ddot{q}_1 & 0\\ (2\ddot{q}_1+\ddot{q}_2)c_2 - \dot{q}_2(2\dot{q}_1+\dot{q}_2)s_2 & \ddot{q}_1c_2 + \dot{q}_1^2s_2\\ \ddot{q}_2 & \ddot{q}_1+\ddot{q}_2\\ \sin q_1 & 0\\ \sin(q_1+q_2) & \sin(q_1+q_2)\end{bmatrix}\end{aligned}$$

$$\begin{aligned}&Y_e(q,f_e)\\ &= \begin{bmatrix}f_{e1}\cos q_1 + f_{e2}\sin q_1 & f_{e1}\cos(q_1+q_2) + f_{e2}\sin(q_1+q_2)\\ 0 & f_{e1}\cos(q_1+q_2) + f_{e2}\sin(q_1+q_2)\end{bmatrix}\end{aligned}$$

In both cases, the authors' tuning of the controllers was respected, considered to be the best possible. Table 1 summarizes the gain parameters used to implement the three controllers.

The initial joint positions and velocities were taken as $q_1(0) = 1$ rad, $q_2(0) = 0.5$ rad, $\dot{q}_1(0) = \dot{q}_1(0) = 0$ rad/s. While the auxiliary states were initiated at $\phi(0) = (2.880.1030.1252.8030.21447.1192.235)^T$ in the case of controller [7], and $\hat{\theta}_d(0) = (2.00.150.1530.01.05)^T$ and $\hat{\theta}_k(0) = (0.50.6)^T$ in the case of controller [15].

The results of the comparative analysis are presented in Figs. 2 and 3 and Table 2. First, in Fig. 2 the impedance or path tracking errors for each controller are depicted; it is possible to observe that in all cases when the interaction force/torque is small (during the first 8 seconds, see Fig. 1) all error components tend to zero. However, when the interaction torque begins to increase, only impedance controllers are able to regulate such human–robot interaction by keeping the error convergence to zero.

On the other hand, the torques generated by all controllers are shown in Fig. 3, where the bounding feature of the pro-

Table 1 Control parameter values

Parameter	JS-IC	JS-TC	TS-IC
k_{P1}	2500	1500	15000
k_{P2}	500	300	15000
k_{D1}	20	20	2000
k_{D2}	5	5	2000
γ_1		20	
γ_2		0.5	
γ_3		0.1	
γ_4		1.5	
γ_5		0.1	
γ_6		10	
γ_7		0.25	
ε		1.0167×10^{-7}	
γ_{k1}			5
γ_{k2}			5
γ_{d1}			30,000
γ_{d2}			0.1
γ_{d3}			5
γ_{d4}			500
γ_{d5}			2.5
λ_{k1}			50
λ_{k2}			50

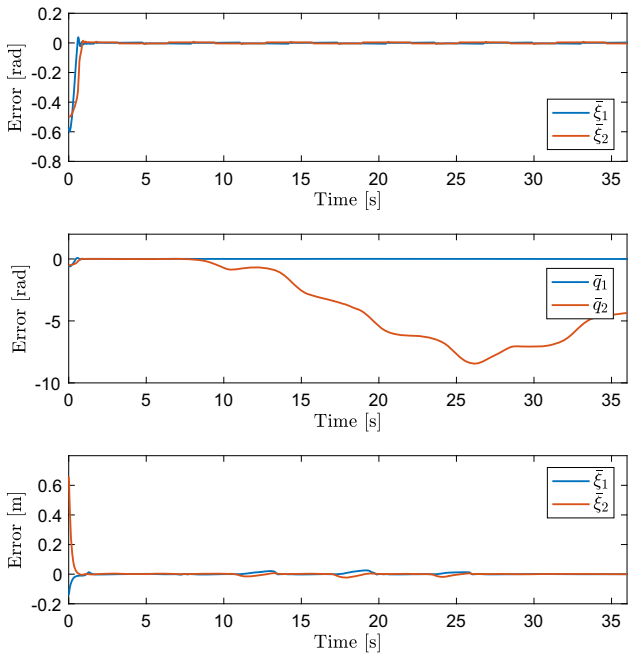

Fig. 2 Components of error for the proposed joint-space impedance controller (JS-IC), the joint-space tracking controller (JS-TC), and the task-space impedance controller (TS-IC), respectively

posed impedance controller (JS-IC) is shown, while for the tracking controller (JS-TC), the torque limit values (200 Nm and 15 Nm, respectively) are not exceeded in both cases. In the graphs on the right, a zoom-in of each torque component is shown, and it can be seen that the Cartesian impedance controller (TS-IC) exceeds the torque limits when starting the movement.

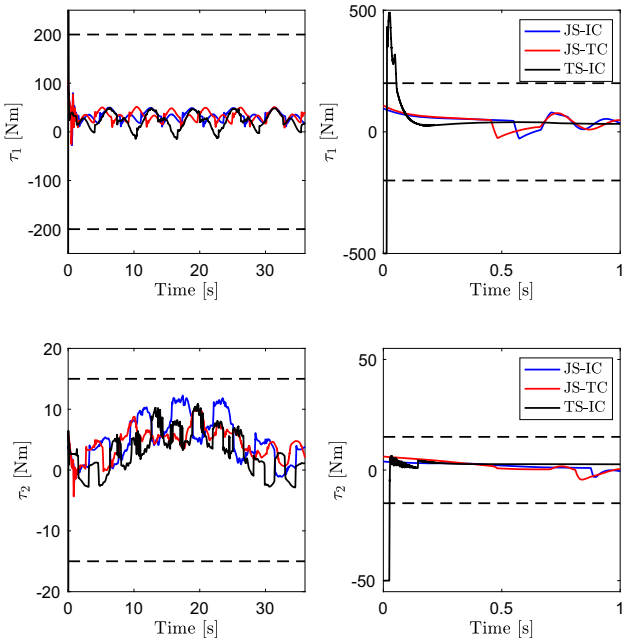

Fig. 3 Applied control torques. The graphs on the right correspond to a zoom-in that allows to appreciate the transient behavior. The segmented lines represent the bounds $\pm T_1$ and $\pm T_2$, respectively

Then, in order to quantify the performance of impedance controllers, the error was normalized with respect to the maximum absolute values of each component (to be able to compare a joint controller with another Cartesian one) and the root-mean-square (RMS) value of the normalized error was calculated as

$$RMS = \sqrt{\frac{1}{T}\int_0^T \|e(t)\|^2 \mathrm{d}t} \tag{60}$$

where $T = 36$ seconds and

$$e(t) = \begin{bmatrix} \bar{\xi}_1(t)/\max_t\{|\bar{\xi}_1(t)|\} \\ \\ \bar{\xi}_2(t)/\max_t\{|\bar{\xi}_2(t)|\} \end{bmatrix} \tag{61}$$

The RMS values of each impedance controller are presented in Table 2, where it can be observed that the values obtained are very similar; however, the performance of the proposed joint-space impedance controller is slightly better and with the advantage of generating bounded control actions (avoiding possible damage to the robot actuators).

From the results obtained in the simulation test and the performance evaluation of the control schemes, the following

Table 2 RMS error values

Index	JS-IC	TS-IC
RMS	0.1476	0.1486

can be stated: (1) the adaptive JS-TC motion control scheme is not robust in the face of disturbances caused by human–robot interaction, especially when the external torque applied by the user is greater than 10% of the maximum value of the actuator, i.e., $|\tau_e(t)| > 1.5$ Nm; (2) the impedance controller TS-IC behaves appropriately when the initial position of the robot is close to the desired trajectory, because it is very sensitive to kinematic singularities. This causes high accelerations which are reflected in the demand for high torques above the actuators' limits, i.e., $\max\{|\tau_1(t)|\} > 15$ Nm and $\max\{|\tau_2(t)|\} > 200$ Nm; (3) although the performance of both impedance controllers (JS-IC and TS-IC) is very similar, our proposal has the advantage of generating bounded torques and because it operates in joint space and is not affected by the kinematic singularities of the robot; (4) our proposal had the best performance since it achieves the convergence of the impedance error toward zero with lower RMS value, respecting the torque limits of the actuators and appropriately regulating the interaction forces exerted by the user. Therefore, the results of this comparative study allow us to conclude that the use of our control scheme in human–robot interaction tasks guarantees a good performance and an adequate level of safety for both the user and the robot.

Finally, another advantage of the proposed control scheme is that the tuning of impedance parameters (K_E, D_E, H_E) allows for bounded modification of the trajectory to be followed by the robot during interaction, i.e., the adjustment vectors of position, velocity and acceleration are bounded if the tuning criterion (16)–(18) is met. Figure 4 depicts the behavior of the trajectory adjustment vectors and shows that the position, velocity, and acceleration do not exceed the bounds $B_{ep} = 0.85$, $B_{ev} = 0.15$, and $B_{ea} = 0.3$, respectively.

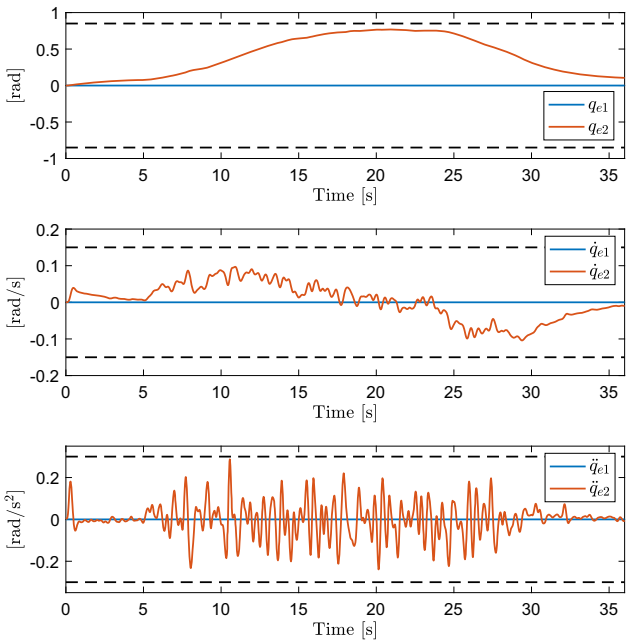

Fig. 4 Torque filter ($\mathcal{F}(s)\tau_e$) outputs q_e, $\dot{q}_e$, and $\ddot{q}_e$, respectively. The segmented lines represent the bounds $\pm B_{ep}$, $\pm B_{ev}$, and $\pm B_{ea}$, respectively

5 Conclusions

Closed-loop stability analysis, physical torque limits of actuators, and sensitivity to singularities are often overlooked in the design of control schemes for safe human–robot interaction tasks. This paper proposes a joint-space impedance controller with bounded actions that makes use of EMG to estimate the user's joint torque during human–robot interaction. The proposed scheme has a nonlinear PD+ structure based on generalized saturation functions and external torque compensation based on EMG and the Hill muscle model. These features respect the torque limits of the actuators and measure the user intent in a more natural way. Moreover, through a Lyapunov stability analysis and numerical simulations, the correct performance of the proposed control scheme was supported and validated. Due to these features, our proposal can be considered as a primary approach to impedance control for safe human–robot interaction with bounded actions.

The results of the comparative tests presented make evident the advantages of the proposed control scheme over other similar controllers to regulate human–robot interaction tasks. This is due to the fact that it can deal with the torques applied by the user at the same time that bounded control actions are generated below the torque limits of the robot's actuators. In addition, the use of Hill's muscle model and EMG for user joint torque estimation allows human–robot interaction to be defined in joint space, preventing the robot from reaching singular configurations as commonly happens with Cartesian controllers.

Acknowledgements This work was supported by the National Council for Science and Technology, Mexico.

Author Contributions Víctor I. Ramírez-Vera contributed to conceptualization, formal analysis, investigation, methodology, and writing—original draft, Marco O. Mendoza-Gutiérrez helped in formal analysis, investigation, supervision, and writing—original draft, and Isela Bonilla-Gutiérrez contributed to investigation, methodology, supervision, and writing—review and editing.

Declarations

Conflict of interest The authors declare that they have no conflict of interest.

References

1. He, W.; Xue, C.; Yu, X.; Li, Z.; Yang, C.: Admittance-based controller design for physical human–robot interaction in the constrained task space. IEEE Trans. Autom. Sci. Eng. **17**(4), 1937–1949 (2020)
2. Xing, H.; Torabi, A.; Ding, L.; Gao, H.; Deng, Z.; Mushahwar, V.K.; Tavakoli, M.: An admittance-controlled wheeled mobile manipulator for mobility assistance: human–robot interaction estimation and redundancy resolution for enhanced force exertion ability. Mechatronics. (2021). https://doi.org/10.1016/j.mechatronics.2021.102497
3. Xie, C.; Yang, Q.; Huang, Y.; Su, S.W.; Xu, T.; Song, R.: A Hybrid arm-hand rehabilitation robot with EMG-based admittance controller. IEEE Trans. Biomed. Circuits Syst. (2021). https://doi.org/10.1109/TBCAS.2021.3130090
4. Taylor, R.H.: A perspective on medical robotics. Proc. IEEE. **94**(9), 1652–1664 (2006)
5. Mendoza, M.; Zavala-Río, A.; Santibàñez, V.; Reyes, F.: Output-feedback proportional-integral-derivative-type control with simple tuning for the global regulation of robot manipulators with input constraints. IET Contr. Theory Appl. **9**(14), 2097–2106 (2015)
6. Aguiñaga-Ruiz, E.; Zavala-Río, A.; Santibàñez, V.; Reyes, F.: Global trajectory tracking through static feedback for robot manipulators with bounded inputs. IEEE Trans. Control Syst. Technol. **17**(4), 934–944 (2009)
7. López-Araujo, D.J.; Zavala-Río, A.; Santibàñez, V.; Reyes, F.: A generalized global adaptive tracking control scheme for robot manipulators with bounded inputs. Int. J. Adapt. Control Signal Process. **29**(2), 180–200 (2015)
8. Hogan, N.; Krebs, H.I.; Charnnarong, J.; Srikrishna, P.; Sharon, A.: MIT-MANUS: a workstation for manual therapy and training. In: Proceedings of IEEE International Workshop on Robot and Human Communication, pp. 161–165 (1992)
9. Krebs, H.I.; Volpe, B.T.; Williams, D.; Celestino, J.; Charles, S.K.; Lynch, D.; Hogan, N.: Robot-aided neurorehabilitation: a robot for wrist rehabilitation. IEEE Trans. Neural Syst. Rehabil. Eng. **15**(3), 327–335 (2007)
10. Nef, T.; Mihelj, M.; Kiefer, G.; Perndl, C.; Muller, R.; Riener, R.: ARMin-Exoskeleton for arm therapy in stroke patients. In: Proceedings of 10th IEEE Int. Conference on Rehabilitation Robotics, pp. 68–74 (2007)
11. Hogan, N.: Impedance control: an approach to manipulation. ASME J. Dyn. Sys. Meas. Control. **107**, 1–24 (1985)
12. Hino, M.; Muramatsu, H: Periodic/aperiodic hybrid position/impedance control using periodic/aperiodic separation filter. In: Proceedings of 2021 IEEE International Conference on Mechatronics, pp. 1–6 (2021)
13. Arnold, J.; Lee, H.: Variable impedance control for pHRI: impact on stability, agility, and human effort in controlling a wearable ankle robot. IEEE Robot. Autom. Lett. **6**(2), 2429–2436 (2021)
14. Zhang, X.; Sun, L.; Kuang, Z.; Tomizuka, M.: Learning variable impedance control via inverse reinforcement learning for force-related tasks. IEEE Robot. Autom. Lett. **6**(2), 2225–2232 (2021)
15. Bonilla, I.; Mendoza, M.; Campos-Delgado, D.U.; Hernández-Alfaro, D.E.: Adaptive impedance control of robot manipulators with parametric uncertainty for constrained path-tracking. Int. J. Appl. Math. Comput. Sci. **28**(2), 363–374 (2018)
16. Li, Z.; Liu, J.; Huang, Z.; Peng, Y.; Pu, H.; Ding, L.: Adaptive impedance control of human–robot cooperation using reinforcement learning. IEEE Trans. Ind. Electron. **64**(10), 8013–8022 (2017)
17. Erchao, L.; Zhanming, L.; Junxue, H.: Robotic adaptive impedance control based on visual guidance. Int. J. Smart Sens. Intell. Syst. **8**(4), 2159–2174 (2015)
18. Liu, C.; He, Y.; Chen, X.; Zhang, X.: Discontinuous force-based robot adaptive switching update rate impedance control. In: Proceedings of the IEEE 5th Advanced Information Technology, Electronic and Automation Control Conference, pp. 2573–2580 (2021)
19. Lakshminarayanan, S.; Kana, S.; Mohan, D.M.; Manyar, O.M.; Then, D.; Campolo, D.: An adaptive framework for robotic polishing based on impedance control. Int. J. Adv. Manuf. Technol. **112**(1), 401–417 (2021)
20. Hu, H.; Wang, X.; Chen, L.: Impedance with finite-time control scheme for robot–environment interaction. Math. Probl. Eng. (2020). https://doi.org/10.1155/2020/2796590
21. Lin, G.; Yu, J.; Liu, J.: Adaptive fuzzy finite-time command filtered impedance control for robotic manipulators. IEEE Access. **9**, 50917–50925 (2021)
22. Sun, T.; Peng, L.; Cheng, L.; Hou, Z.G.; Pan, Y.: Stability-guaranteed variable impedance control of robots based on approximate dynamic inversion. IEEE Trans. Syst. Man Cybern. Syst. **51**(7), 4193–4200 (2019)
23. Hamedani, M.H.; Zekri, M.; Sheikholeslam, F.: Adaptive impedance control of uncertain robot manipulators with saturation effect based on dynamic surface technique and self-recurrent wavelet neural networks. Robotica. **37**(1), 161–188 (2019)
24. Arefinia, E.; Talebi, H.A.; Doustmohammadi, A.: A robust adaptive model reference impedance control of a robotic manipulator with actuator saturation. IEEE Trans. Syst. Man Cybern. Syst. **50**(2), 409–420 (2017)
25. Rodríguez-Liñán, M.; Mendoza, M.; Bonilla, I.; Chávez-Olivares, C.: Saturating stiffness control of robot manipulators with bounded inputs. Int. J. Appl. Math. Comput. Sci. **27**(1), 79–90 (2017)
26. Maldonado-Fregoso, B.; Mendoza-Gutierrez, M.; Bonilla-Gutierrez, I.; Vidrios-Serrano, C.: A generalized adaptive stiffness control scheme for robot manipulators with bounded inputs. Asian J. Control. **23**(6), 2550–2564 (2021)
27. Peng, L.; Hou, Z. G.; Wang, W.: A dynamic EMG-torque model of elbow based on neural networks. In: Proceedings of the 37th Annual International Conference of the IEEE Engineering in Medicine and Biology Society, pp. 2852–2855 (2015)
28. Li, Z.; Huang, Z.; He, W.; Su, C.Y.: Adaptive impedance control for an upper limb robotic exoskeleton using biological signals. IEEE Trans. Ind. Electron. **64**(2), 1664–1674 (2016)
29. Khoshdel, V.; Akbarzadeh, A.; Naghavi, N.; Sharifnezhad, A.; Souzanchi-Kashani, M.: sEMG-based impedance control for lower-limb rehabilitation robot. Intell. Serv. Robot. **11**(1), 97–108 (2018)
30. Roveda, L.; Piga, D.: Sensorless environment stiffness and interaction force estimation for impedance control tuning in robotized interaction tasks. Auton. Robot. **45**(3), 371–388 (2021)
31. Mendoza, M.; Bonilla, I.; Reyes, F.; González-Galván, E.: A Lyapunov-based design tool of impedance controllers for robot manipulators. Kybernetika. **48**(6), 1136–1155 (2012)
32. Han, J.; Ding, Q.; Xiong, A.; Zhao, X.: A state-space EMG model for the estimation of continuous joint movements. IEEE Trans. Ind. Electron. **62**(7), 4267–4275 (2015)
33. Khalil, H.K.: Nonlinear Systems, 3rd edn Prentice Hall, Upper Saddle River (2002)
34. Mendoza, M.; Zavala-Río, A.; Santibáñez, V.; Reyes, F.: A generalised PID-type control scheme with simple tuning for the global

regulation of robot manipulators with constrained inputs. Int. J. Control. **88**(10), 1995–2012 (2015)
35. Vidrios-Serrano, C.; Mendoza, M.; Bonilla, I.; Maldonado-Fregoso, B.: A generalized vision-based stiffness controller for robot manipulators with bounded inputs. Int. J. Control Autom. Syst. **19**(1), 548–561 (2021)
36. Kelly, R.; Santibáñez, V.; Loría, J.A.: Control of Robot Manipulators in Joint Space. Springer, London (2006)
37. Ding, Q.; Xiong, A.; Zhao, X.; Han, J.: A novel EMG-driven state space model for the estimation of continuous joint movements. In: Proceeding of the 2011 IEEE International Conference on Systems, Man and Cybernetics, pp. 2891–2897 (2011)
38. Reyes, F.; Kelly, R.: Experimental evaluation of identification schemes on a direct drive robot. Robotica **15**(5), 563–571 (1997)
39. Wiedemann, L.; Ward, S.; Lim, E.; Wilson, N.; Hogan, A.; Holobar, A.; McDaid, A.: Dataset on isometric contractions of the elbow joint in children with and without spastic Cerebral Palsy: HD-EMG and torque. Mendeley Data, V1 (2019). https://doi.org/10.17632/599rgxhy6m.1